remote sensing

MDPI

Article

Effect of Lockdown Measures on Atmospheric Nitrogen Dioxide during SARS-CoV-2 in Spain

Francisco-Javier Mesas-Carrascosa *, Fernando Pérez Porras, Paula Triviño-Tarradas, Alfonso García-Ferrer and Jose Emilio Meroño-Larriva

Department of Graphic Engineering and Geomatics, Campus de Rabanales, University of Cordoba, 14071 Córdoba, Spain; o12pepof@uco.es (F.P.P.); ig2trtap@uco.es (P.T.-T.); agferrer@uco.es (A.G.-F.); ir1melaj@uco.es (J.E.M.-L.)

* Correspondence: fjmesas@uco.es

Received: 1 June 2020; Accepted: 8 July 2020; Published: 10 July 2020

Abstract: The disease caused by SARS-CoV-2 has affected many countries and regions. In order to contain the spread of infection, many countries have adopted lockdown measures. As a result, SARS-CoV-2 has negatively influenced economies on a global scale and has caused a significant impact on the environment. In this study, changes in the concentration of the pollutant Nitrogen Dioxide (NO_2) within the lockdown period were examined as well as how these changes relate to the Spanish population. NO_2 is one of the reactive nitrogen oxides gases resulting from both anthropogenic and natural processes. One major source in urban areas is the combustion of fossil fuels from vehicles and industrial plants, both of which significantly contribute to air pollution. The long-term exposure to NO_2 can also cause severe health problems. Remote sensing is a useful tool to analyze spatial variability of air quality. For this purpose, Sentinel-5P images registered from January to April of 2019 and 2020 were used to analyze spatial distribution of NO_2 and its evolution under the lockdown measures in Spain. The results indicate a significant correlation between the population's activity level and the reduction of NO_2 values.

Keywords: nitrogen dioxide; SARS-Cov-2; Sentinel-5P; air pollution

1. Introduction

Clean air is an essential requirement for human health, and as such air pollution is a major threat to human well-being. Air pollution is the largest environmental health risk in many regions around the world. The World Health Organization estimates that air pollution kills 7 million people worldwide every year, making it necessary to monitor air pollution and improve air quality [1]. The environmental impact is more evident in areas where population density is high, being particularly severe in megacities where high population density, extensive motor vehicle use and strong industrial expansion are combined [2]. Poor air quality is not exclusive to megacities; even small cities with populations around 150,000 can have this problem [3]. Therefore, the economic development of cities with expanding industrial areas is associated with increasing population size and environmental degradation of the surrounding areas [4]. In addition, the high levels of motor vehicle activity [5] and their inappropriate use [6] cause an increase of air pollutants in city centers [7]. As a result, quality of life and human health is worsening specifically in cardiovascular, neurological, and respiratory diseases [8–10] and even results in higher mortality rates [11,12]. As a consequence of this, developed and developing countries are more and more attentive to urban air quality, developing guidelines, directives and standards to inform and support policymakers [13,14] to reduce the health impacts of air pollution.

Common pollutants in the troposphere, the innermost layer of Earth's atmosphere, include ozone (O_3), carbon monoxide (CO), sulfur dioxide (SO_2), nitrogen dioxide (NO_2) and aerosols. NO_2, specifically, has been correlated with mortality in studies in different parts of the world [15,16]. It is true, however, that there is no clear evidence to establish that NO_2 acts as an independent agent causing increases in the mortality rate [17]. Rather, it is widely believed that NO_2 could act as a substitute component for others that are not currently being monitored or, more broadly, as a mixture of pollutants [18]. The result is that NO_2 is included in the multi-pollutant health indexes [19]. Epidemiological research and studies have shown how NO_2 is related to adverse health effects like lung cancer [20,21], asthma exacerbations [22,23] and cardiopulmonary mortality [24,25]. Mainly, NO_2 forms from ground-level emissions caused by the burning of fossil fuels from industrial sources, vehicles and power plants. It contributes to ground-level ozone formation and it is linked to negative effects on respiration. For example, NO_x reacts with moisture, ammonia and other compounds to form small particles that can penetrate into sensitive parts of the lungs.

Traditionally, air pollution is monitored using a networks of sensors, such as gas chromatograph-mass spectrometers [26] or ultraviolet sensors [27], among others, which are distributed over a territory and provide quality information on a wide range of pollutants. The traditional instrumentation used for air quality monitoring is expensive, large, location dependent and yields extremely low spatial and temporal resolution [28]. For this reason, portable environmental sensor systems have been developed using Wireless Sensor Network technology at a lower cost, offering data with a higher frequency over time. They are also easier to relocate and provide better coverage of the area of interest due to allowing the use of a larger number of nodes [29,30], permitting the development of more efficient and accurate air quality models [31]. Despite these advantages, however, it is not possible to map a broad region. Advances in atmosphere remote sensing have opened new avenues for measuring and monitoring atmospheric pollution at local, regional, continental or global scales [32], providing new challenges and opportunities for environmental health research [33]. The ability to observe and monitor air pollutants from sensors onboard satellite platforms has improved in the last two decades. From the first ultraviolet-visible spectrometer, the Global Ozone Monitor Experiment (GOME), with a spatial resolution equal to 40×320 km^2 [34], followed by the SCanning Imaging Absorption SpectroMeter for Atmospheric CHartography (SCIAMACHY), with a pixel size of 30×60 km^2 [35], and GOME-2, 40×80 km^2 [36] to the Ozone Monitoring Instrument, 13×24 km^2 [37] it has been possible to study the distribution of pollutants at urban scales. Recently, the European Space Agency launched the Sentinel-5 Precursor (S5P) to provide data on air quality, the climate and the ozone layer using the TROPOspheric Monitoring Instrument (TROPOMI) as its payload [38] providing a significant improvement in data quality and spatial resolution now at 7×7 km^2 [39]. The spectral bands of the spectrometer TROPOMI ranges from ultraviolet, visible, near infrared and shortwave infrared, allowing the observation of the prevalence of aerosols in the atmosphere, cloud characteristics, concentrations of carbon monoxide (CO), formaldehyde (CH_2O), nitrogen dioxide (NO_2), ozone (O_3), sulphur dioxide (SO_2) and methane (CH_4). The Tropospheric Vertical Column Density (VCD) data of these components are measured from space by sensors like TROPOMI which serves as an accurate proxy at ground level in many air quality applications [40]. The VCD is defined as the number of molecules of a certain atmospheric gas between the on-board sensor of the satellite platform and the Earth's surface per unit area. Tropospheric and stratospheric column densities are separated using a data assimilation system based on the three-dimensional global Tracer chemical Transport Model (TM5-MP), after which they are converted to VCD by a look-up table of altitude dependent air-mass factors and information on the vertical distribution of NO_2 [41]. For NO_x, VCD measurements have been successfully used to estimate trends and variations in atmospheric concentration [42,43], infer surface emissions [44,45] and monitor emission changes at a given location [46,47].

Since mid-February 2020, all efforts of many countries were directed towards combating SARS-CoV-2. However, at the beginning of 2020, the risk of a pandemic from a virus was not among the perceived risks worldwide. This year was the first time that the World Economic Forum's Global

Risk Report showed how climate change and environmental risks were among the top positions [48]. However, both problems are associated, the origin of new pathogens, such as SARS-CoV-2, may be explained by environmental degradation. The coronaviruses have been known about since 1930 [49]. They are transmitted from animals [50] and have been increasing in number over the last decades [51]. The degradation of natural spaces from human activity is increasing the rate of contact between wild spaces and humans, resulting in new diseases and facilitating their expansion [52–54]. Nevertheless, while many believe that the climate, and therefore the environment is changing, some think this is not attributable to human activity [55], which may be due to their perception of cultural values [56] or ideologically and politically motivated actors [57].

Unfortunately, the spread of the coronavirus SARS-Cov-2 has been unstoppable and has become a pandemic [58], with dramatic results in countries like Spain, Italy and the United Kingdom [59] in Europe's case. Interventions like quarantine or isolation have shown to be effective in reducing the number of SARS-CoV-2 infections [60]. In addition, some countries and regions have deemed it necessary to impose lockdown measures on economic activities and with unprecedented travel restrictions [61,62]. Under this lockdown period, changes in air pollution can provide valuable information on air quality improvement when there are restrictions on emissions. In this manuscript, using Sentinel S5P images, we analyze the spatial and temporal variation of NO_2 concentrations during Spain's SARS-Cov-2 lockdown phase which took place in March and April 2020, and how these variations are related to city-scale demographics.

2. Materials and Methods

2.1. Study Area

Spain has just over 47 million inhabitants as of 1 January 2020. Although unevenly distributed throughout the territory, the average population density is equal to 82 habitants per km^2. Figure 1 shows population density using the European Environment Agency 10 × 10 km grid as a reference. There are areas with highly concentrated populations next to areas of demographic voids. The factors that explain this unbalanced population distribution in Spain are both natural and historical. Regarding natural factors areas with flat and low-lying relief, with a temperate and humid climate and access to the sea and rivers are the most populated. As far as historical factors are concerned, the distribution of the population is related to the economic structure of the country and the development of transport and communication infrastructure. As a result, the average population density in Spain is 416 inhabitants per square kilometer, with very high density areas, over 750 habitants per square kilometer, compared to others with very low densities.

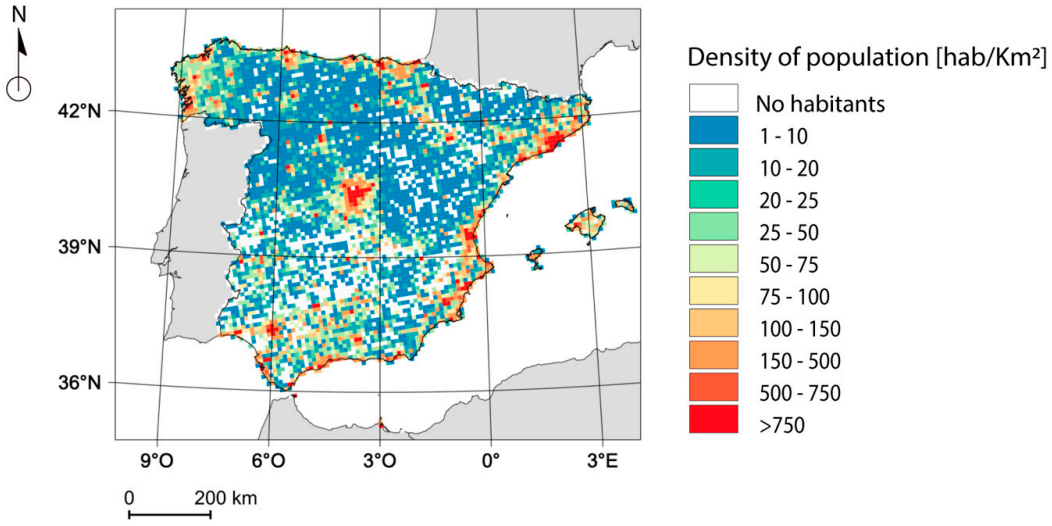

Figure 1. Distribution of population density in Spain on a 10 × 10 km grid.

Figure 2 shows the location of cities with more than 275,000 inhabitants, with the highest concentrations in Madrid, having more than 3 million inhabitants, and Barcelona, with just over 1.6 million. The relationship between the number of inhabitants in these eleven cities and the variation of NO_2 VCD under the lockdown measures is the focus of this analysis.

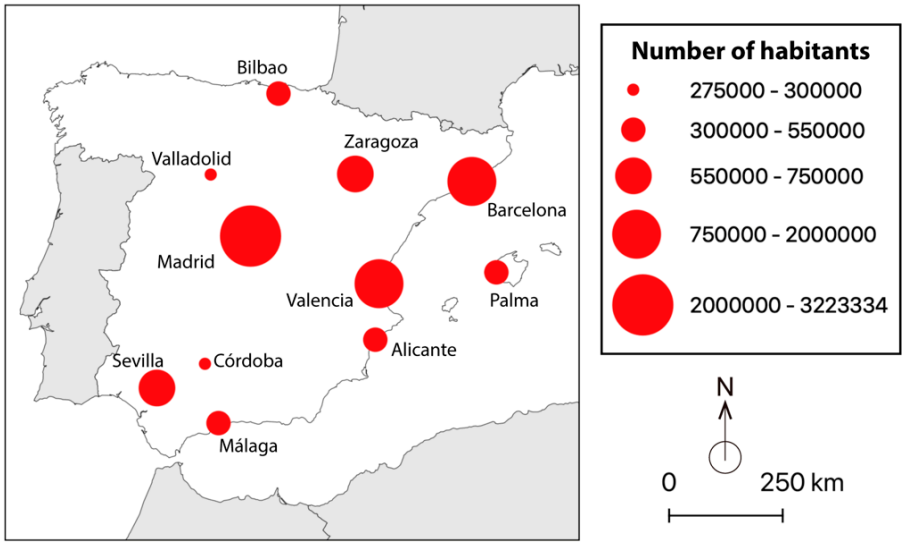

Figure 2. Location of the eleven most populated cities in Spain.

2.2. Remote Sensing Image Collections

The TROPOMI on-board the Sentinel-5 Precursor (Sentinel-5P) was used to collect data on NO_2 concentration. The Sentinel-5P mission, launched by the European Space Agency in 2017, is a low-orbit polar satellite used to monitor Earth's atmosphere with a high spatio-temporal resolution using the TROPOMI. Concretely, it is a multispectral sensor that registers reflectance values at ultraviolet-visible (250–500 nm), near-infrared (675–775 nm) and short-wave infrared (2305–2385 nm) wavelengths which measures concentrations of ozone, methane, formaldehyde, aerosols, carbon monoxide, nitrogen oxide and sulphur dioxide as well as cloud characteristics like cloud fraction, cloud base and pressure.

Image processing was performed with the Google Earth Engine, a cloud-based platform for geospatial analysis with high computational capabilities [63]. A total of 1637 Sentinel 5P Nitrogen Dioxide level-3 scenes of Spain from January to April of 2019 were used and 1636 scenes from the same period were used from 2020 (Table 1). Thus, Sentinel 5P Level-2 data [64] are processed to obtain a single grid per orbit, which allows the Google Earth Engine to process the data. In addition, the data are previously filtered, resulting in pixels with quality assurance values less than 75% being removed, such as cloud or partially snow-covered pixels, errors and or problematic retrievals. First, for each month and year a median image was generated to represent the time series of the images, obtaining an individual image for each time period. Thus, each pixel in the output image was equal to the median value of all the images at that location. On the NO_2 median images, once masked for the geographical space of Spain, the statistics corresponding to maximum, minimum, median, and 2nd and 3rd quartile were determined. This allowed a space-time comparison of the NO_2 VCD throughout the year and between years.

In addition, the variation of NO_2 VCD before and after the lockdown measures was determined. Thus, taking 15 March 2020 as a time reference, the day on which the lockdown measures became effective in Spain, a median image was calculated to represent the NO_2 VCD one month before and after the adoption of these measures, and the variation of this component was then determined. For the most populated cities in Spain, the average value of variation of NO_2 VCD was determined in order to analyze its relationship with the number of inhabitants per city.

Table 1. Number of Sentinel-5P scenes used per month and year.

Month	2019	2020
January	426	424
February	382	379
March	426	426
April	403	407
Total	1637	1636

3. Results

European countries have established differing lockdown measures in order to control the spread of the SARS-CoV-2 outbreak. These measures, imposed at varying degrees, were implemented at different moments during the second half of March 2020 and have restricted freedom of movement and outlawed public meetings. Italy and Spain were the first countries in Europe to implement these measures on 11 and 14 March 2020, respectively. Taking 15 March 2020 as a time reference, Figure 3 shows the evolution of NO_2 VCD in the troposphere at a European scale one month before and after the adoption of the lockdown measures and compares it to the concentration in the same period during the year 2019. At this scale of detail, it can be seen that the highest NO_2 VCD distribution values appears in central Europe, large European cities and some urban areas of the Mediterranean basin. One month before 15 March, both in 2019 (Figure 3a.I) and 2020 (Figure 3b.I), the regional distribution of the average NO_2 VCD around Milan, Paris, Madrid, London showed values higher than 0.0002 mol m^{-2}. Likewise, between 15 March and 15 April 2019 (Figure 3a.II), NO_2 VCD distribution was maintained around the previously described urban areas. However, for the same period in 2020 (Figure 3b.II) these extreme values greatly declined, coinciding with the lockdown period.

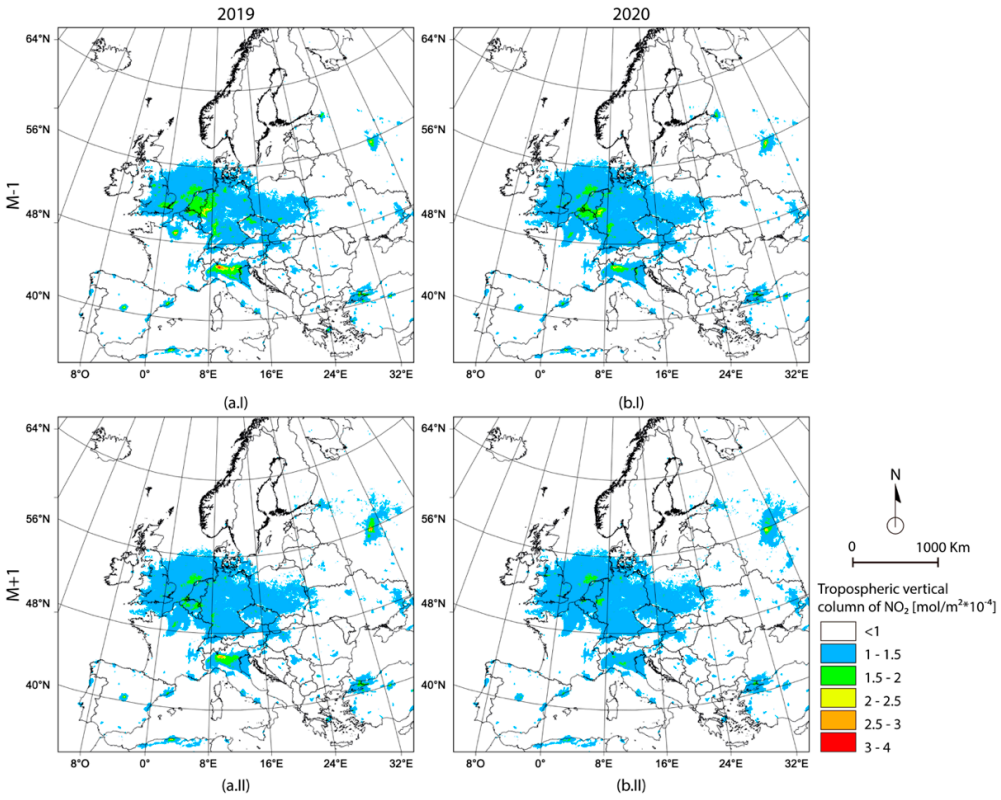

Figure 3. Comparison in Europe of the evolution of the average NO_2 content in the troposphere one-month (**I**) before and (**II**) after March 15, (**a**) 2019 and the same period in (**b**) 2020.

Figure 4 shows the box and whisker plot and Table 2 the statistic description of NO_2 VCD in Spain for 2019 and 2020 from January to April. A wide range of NO_2 VCD values were observed (Figure 4a), especially in January and February of both years. The maximum values were reduced in March and April, especially in 2020, and declined sharply in April 2020, coinciding with mobility restrictions. On the other hand, the minimum values did not fluctuate, maintaining similarity throughout the months of both years. Median, quartile 25% and 75% values were closer to the minimum values, showing the presence of geographical areas with higher values of NO_2 VCD than the rest. Figure 4.a shows how the range of NO_2 was reduced in March and April in the two years. However, while in 2019 the distribution was very similar, this was not the case in 2020. In March 2020, the reduction in the range of NO_2 VCD was more pronounced than in the same month of the previous year. In April 2020, the reduction was much more pronounced, coinciding with mobility restrictions. Figure 4b shows in detail the evolution of the distribution of NO_2 VCD around the median values. During 2019, the median values were similar, ranging from 2.08×10^{-5} to 2.19×10^{-5} mol m^{-2} in January and February, respectively. Contrariwise, in 2020, the median values of NO_2 did not show the same stable behavior of the previous year. January 2020 showed the highest value, 2.75×10^{-5} mol m^{-2}, reducing slightly in February, although it was still higher than the previous year's values. However, in the month of March 2020 there was a very pronounced reduction of NO_2 in April 2020, with a median value equal to 1.65×10^{-5} mol m^{-2}, the lowest value of all the months analyzed. In addition, the interquartile range in the months of March and April 2020 was smaller and therefore the distribution of NO_2 was more homogeneous throughout the territory.

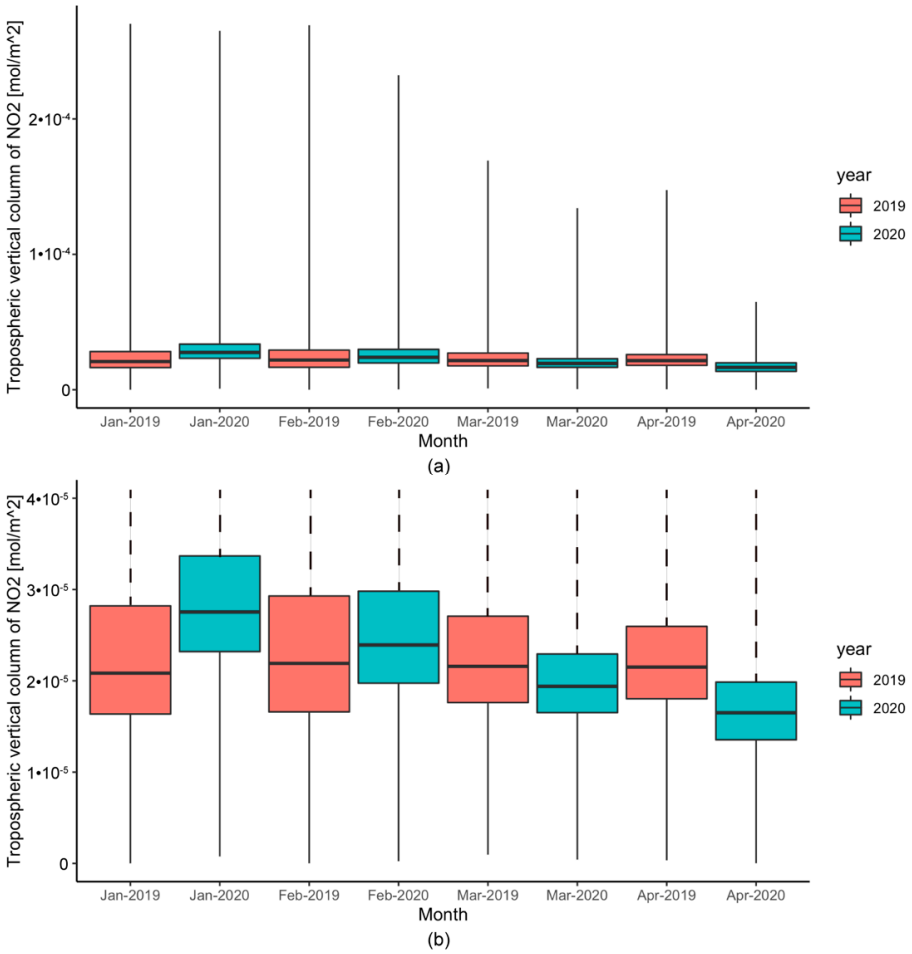

Figure 4. Whisker box plot with the monthly evolution of NO_2 in 2019 and 2020 taking into account (**a**) the whole range of values and (**b**) zoom on the median values.

Table 2. Descriptive statistics of NO_2 concentration by month and year.

Month	Year	Minimum	Maximum	Q25	Median	Q75
January	2019	1.46×10^{-9}	0.00027	1.64×10^{-5}	2.08×10^{-5}	2.82×10^{-5}
	2020	7.63×10^{-7}	0.000265	2.32×10^{-5}	2.75×10^{-5}	3.37×10^{-5}
February	2019	7.41×10^{-9}	0.000269	1.66×10^{-5}	2.19×10^{-5}	2.93×10^{-5}
	2020	2.4×10^{-7}	0.000232	1.97×10^{-5}	2.39×10^{-5}	2.98×10^{-5}
March	2019	9.56×10^{-7}	0.000169	1.76×10^{-5}	2.16×10^{-5}	2.71×10^{-5}
	2020	4.12×10^{-7}	0.000134	1.65×10^{-5}	1.94×10^{-5}	2.29×10^{-5}
April	2019	3.32×10^{-7}	0.000148	1.8×10^{-5}	2.15×10^{-5}	2.6×10^{-5}
	2020	1.25×10^{-8}	6.49×10^{-5}	1.35×10^{-5}	1.65×10^{-5}	1.99×10^{-5}

Figure 5 shows the temporal evolution of the spatial distribution of NO_2 VCD in the January–April period for the years 2019 and 2020 in Spain. During the year 2019 (Figure 5I), Madrid and the surrounding metropolitan area was the one with the highest values of NO_2 VCD. In addition, the metropolitan areas of Barcelona and Valencia, in the Mediterranean basin, and Seville in southern Spain, stand out in NO_2 VCD values, although much lower than Madrid. These areas correspond to the areas with the highest NO_2 VCD values represented in the box and whisker plot of Figure 4a. As shown in this figure, these urban areas appear more highlighted in the months of January (Figure 5I.a) and February (Figure 5I.b) than in the months of March (Figure 5I.c) and April (Figure 5I.d) in 2019, although these areas presented higher values than the rest of Spain. In 2020 (Figure 5II), the distribution of NO_2 VCD was similar to that of 2019 in the months of January (Figure 5II.a) and February (Figure 5II.b), with the same urban areas standing out as in 2019 due to their increase in NO_2. In March 2020, coinciding with the middle of the month in which mobility restriction measures were adopted, a reduction in NO_2 VCD was observed throughout the country, with only the geographical area around Madrid showing higher values than the rest of Spain, although lower than in previous months. Finally, in April 2020 (Figure 5II.d), where the mobility restrictions measures were applied throughout the month, there was a very marked reduction in NO_2 VCD throughout the totally of Spain, with strongly homogeneous behavior and hardly any variation.

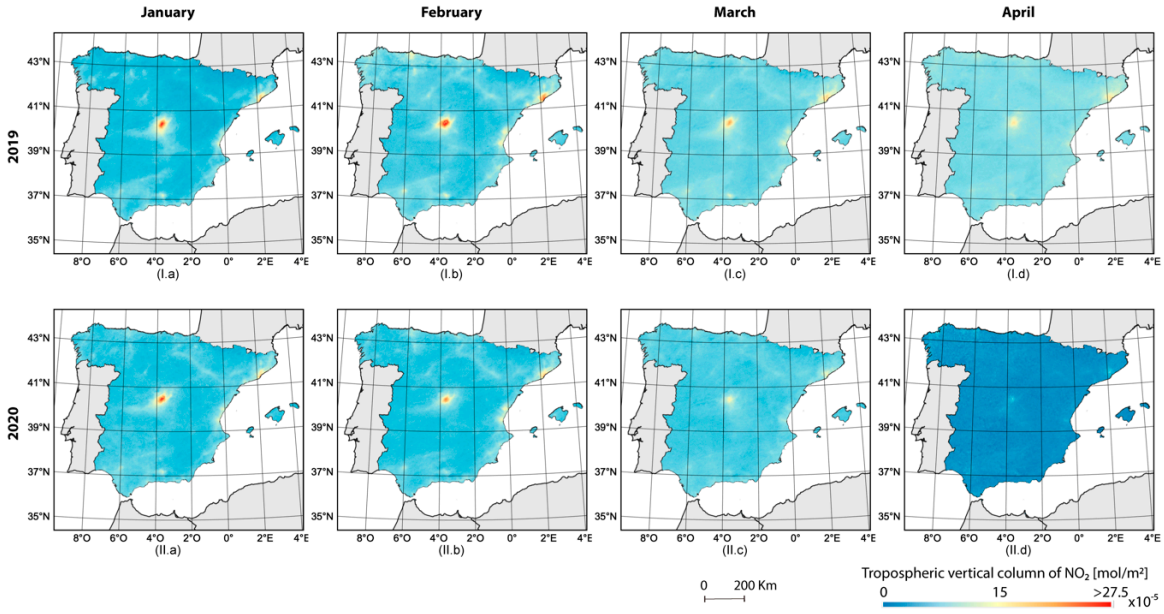

Figure 5. Monthly maps of average values of Tropospheric vertical column of NO_2 in Spain for the years (**I**) 2019 and (**II**) 2020 during the months of (**a**) January, (**b**) February, (**c**) March and (**d**) April.

Figure 6 presents the evolution in detail of NO_2 VCD over the three most populated cities in Spain, Madrid (Figure 6a), Barcelona (Figure 6b) and Valencia (Figure 6c), between January and April 2020. Of the three cities, Madrid presented the highest NO_2 VCD values at the beginning of 2020. In the month of January, both Madrid (Figure 6a.I) and Barcelona (Figure 6b), due to the size of their metropolitan areas and number of inhabitants, showed higher values in the center of these areas, reducing radially as the distance increases from the central area. In February, there was a reduction in NO_2 in the city of Madrid (Figure 6a.II), but not in the cities of Barcelona (Figure 6b.II) and Valencia (Figure 6c.II). These geographical areas presented higher values than the surrounding areas. In March, coinciding with the limitation of mobility and activity in the middle of the month, a reduction in NO_2 was observed in the three urban areas. In the case of Madrid (Figure 6a.III), the highest NO_2 values appeared around the city and not in the metropolitan area. A similar NO_2 spatial distribution occurred in Barcelona (Figure 6b.III). On the other hand, the city of Valencia and its metropolitan area (Figure 6c.III) present very similar NO_2 values. The effect of mobility restrictions is very evident in the month of April 2020. All analyzed urban areas showed a drastic decrease in NO_2 VCD, only Madrid (Figure 6a.IV) and, to a lesser extent, Barcelona (Figure 6b.IV) showed a very slight increase in values with respect to the surrounding areas for the same period, making it practically impossible to identify a pattern associated with the urban area. In the case of Valencia (Figure 6c.IV) this difference vanished completely. Thus, after 30 days of limitations and restrictions in mobility and activity, the values of NO_2 CDV in these urban areas were similar to those of non-urban areas.

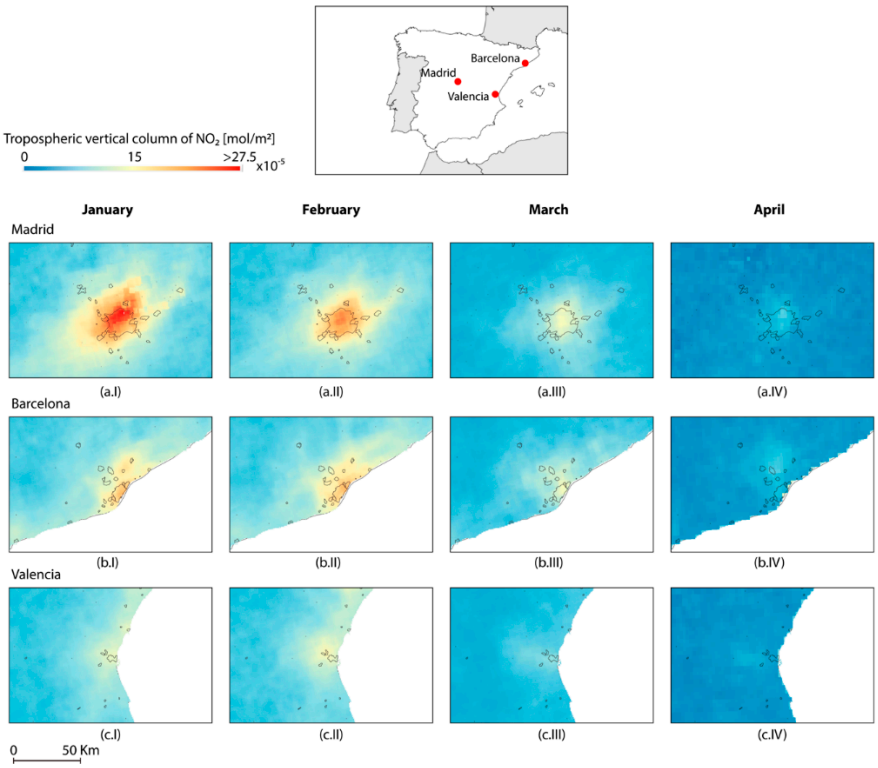

Figure 6. Monthly maps of average values of Tropospheric vertical column of NO_2 in (**a**) Madrid, (**b**) Barcelona and (**c**) Valencia for 2020 during the months of (**I**) January, (**II**) February, (**III**) March and (**IV**) April.

Figure 7 shows the variation of NO_2 VCD from one month before to one month after 15 March 2020 in Spain. The highest NO_2 VCD reductions are represented in red, while a severe reduction is represented in yellow. On the other hand, those areas with a low reduction are represented in green and those areas with no discernible variation are in cyan. Throughout the territory, a decrease can be observed after the lockdown measures, with some areas showing a more pronounced decrease

than others. The variation of NO_2 followed the same spatial distribution as the population density distribution presented in Figure 1. The city of Madrid, the most densely populated city in Spain, showed a marked reduction in NO_2 concentration, reaching values of -1.56×10^{-4} mol m^{-2}. Slightly lower values were found in areas such as Barcelona, Valencia and some coastal urban areas with a lower population density than Madrid. On the other hand, all these areas were surrounded by metropolitan areas where the reduction in NO_2 was much less pronounced but also important, with values around -0.08×10^{-4} mol m^{-2}. Similar values were found in cities such as Seville and its metropolitan area, Valladolid and the Ebro River corridor. The rest of the territory, with lower population densities presented a reduction between 0.04×10^{-4} and 0.01×10^{-4} mol m^{-2}, lower than metropolitan areas. Therefore, the most densely populated areas with high NO_2 concentrations showed the greatest reductions compared to those areas with low density populations. As a result, the distribution of NO_2 VCD in Spain was more homogeneous than in previous months (Figure 5II.d).

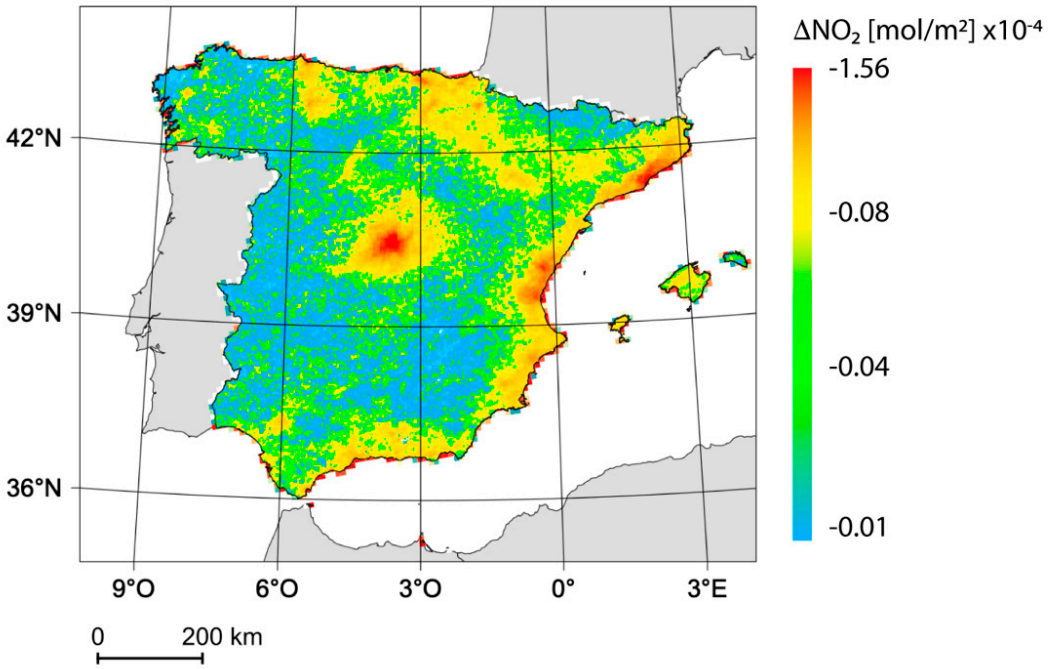

Figure 7. Mean variation of NO_2 VCD between one month before and after 15 March 2020 in Spain.

Figure 8 shows the average value of tropospheric VCD of NO_2 reduction in relation to the number of inhabitants, resulting in nine categories. In general, as the number of inhabitants increases, NO_2 decreases. Cities with less than 50,000 inhabitants had least significant reduction, with an average value of -2.99×10^{-5} mol m^{-2}. On the other hand, those cities with more than 600,000 inhabitants were those that presented the greatest reduction, with average values of less than -1.05×10^{-4} mol m^{-2}. Considering the first three categories with the lowest number of inhabitants, the factor of increase in the reduction of tropospheric VCD of NO_2 was equal to 1.28 per 50,000 inhabitants. On the other hand, it decreased slightly among the categories of 150,000 to 600,000 inhabitants, being equal to 1.03 per 50,000 inhabitants.

The 11 cities with more than 275,000 inhabitants in Spain, are plotted in Figure 9 which shows a negative lineal relationship between population size and NO_2 reduction with a correlation coefficient equal to 0.73 (p-value 0.00004). A negative relationship was expected between population activity and NO_2 levels, where greater activity leads to a higher level. This component is one of the most important in urban air pollution, with the burning of fossil fuels such as coal, oil and gas being one of the main sources of NO_2. It is estimated that about 86% of nitrogen dioxide in European cities are caused by fossil fuels emitted from motor vehicles [65]. That means that as populations increase,

NO_2 also increases. With the lockdown measures in effect there has been almost no vehicle traffic and in turn the concentration of NO_2 has been reduced.

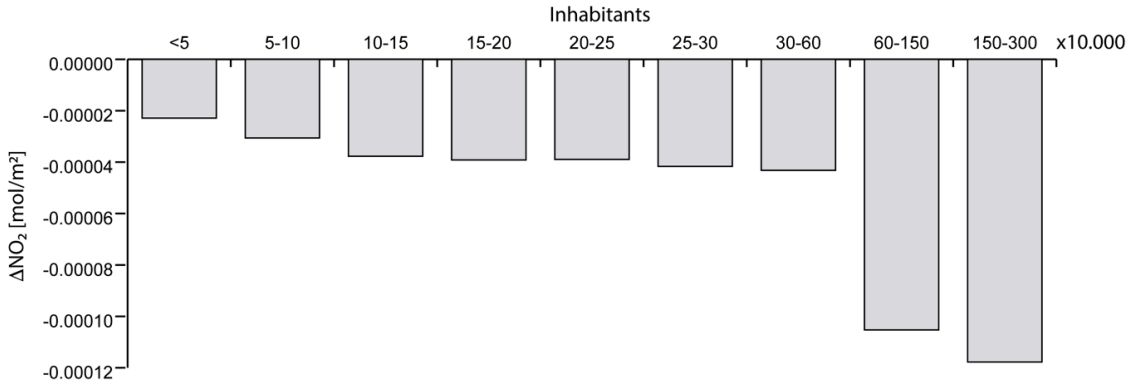

Figure 8. Number of inhabitants versus variation of tropospheric vertical column of NO_2.

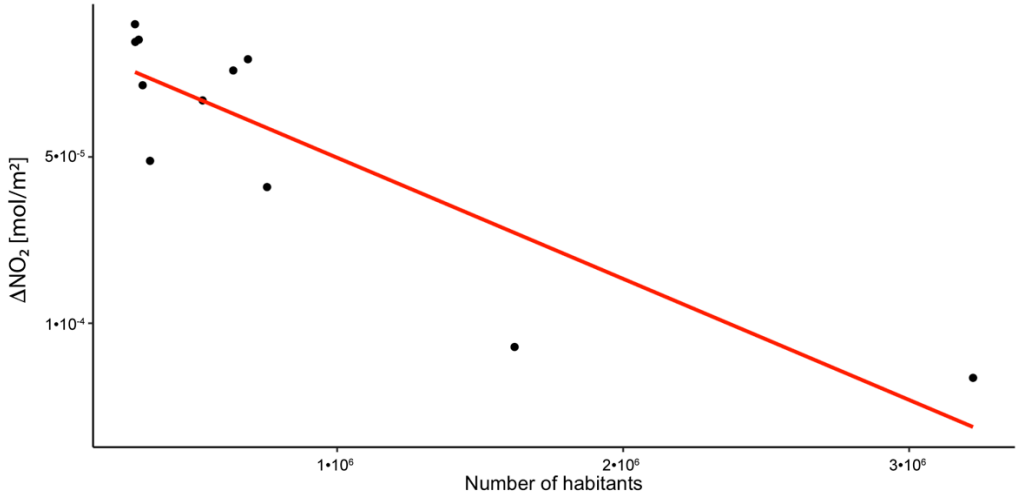

Figure 9. Number of inhabitants versus variation of tropospheric vertical column of NO_2. The red line is the fitted linear function.

4. Discussion

NO_2 concentrations in megacities exceed recommendations from the World Health Organization [13]. To control the spread of coronavirus the large majority of people have been staying at home, maintaining social distancing practices and working remotely [66]. As expected, the direct consequence of industries and transportation systems shutting down was a sudden drop in air pollutant emissions. The lockdowns have provided researchers the opportunity to set up singular experiments based on real data and not simulations to answer the question of what would happen if individual transport based on fuel combustion were removed and only those linked to public service and supply were active. Under this scenario, around the world, many cities have looked into how air quality has improved since the lockdown measures took place. Particularly in Europe, NO_2 emissions were highly reduced over northern Italy, Spain and the United Kingdom [67]. It is well known there is a positive association between NO_2 concentration and population size [68]. As in other studies in other countries [69], in Spain, NO_2 concentrations are located around urban areas, being higher as population size increases, indicating anthropogenic sources, mainly produced by vehicles. The situation caused by the SARS-CoV-2 pandemic has led, in the case of Spain, to an 80% reduction in traffic and a reduction of fuel sales by 83% [70].

Urban planners, engineers and policymakers should take the studies that have capitalized on the unique conditions presented by the pandemic into account to promote new strategies to reduce air pollution and consolidate existing ones. To this end, it is necessary to consider how the expansion of urban areas and the complex use of land, transport patterns and socio-economic development directly factor into our living conditions. The expansion of urban areas has led to an increase in residential areas on the outskirts of cities, resulting in disproportionate distances between residential housing and places of work, generating an imbalance in transport with a high dependence on private vehicles [71]. To date, there is not a sufficient number of studies taking into account the integration of transport systems and urban planning to reduce air pollution [72,73].

Regardless of the positive impact on the reduction of air pollutants, climate effects are still present today and should not be understood as a substitute for climate change. In this way, we would like to express that in this manuscript we characterized the changes produced on air quality during the lockdown. We have not tried to attribute specifically nor quantify the effects of the lockdown since other factors may have influenced the changes, such as meteorology and regional and long-range transport of pollutants. An in-depth analysis is required to obtain this information accurately.

In addition to the impact of lockdown measures on air quality, future work should aim to study the impact of the absence of tourists on the appearance of beaches and water quality, or the reduction of noise pollution. Moreover, the massive use of personal protective equipment such as masks or gloves has increased worldwide, and probably recycling and waste management policies should be analyzed and redesigned.

5. Conclusions

Lockdown measures due to SARS-CoV-2 have provoked a singular and unique opportunity to evaluate the contribution and impact of human activity on the environment. In this manuscript, the effect on air pollution due to the pandemic response in Spain has been shown by evaluating and analyzing the concentration of tropospheric NO_2 from 1 January to 30 April in 2019 and 2020. In this study, data from the TROPOMI on-board the Sentinel-5P satellite platform were used to analyze the spatial-temporal variation in Spain and its relationship with population size and lockdown measures.

The satellite scenes showed a high concentration of NO_2 in the city of Madrid, which has the largest number of inhabitants in Spain. Other hotspots with high concentrations of NO_2 also appeared over cities with a large number of inhabitants. Previous lockdown measures, the relationship between the population density map of Spain and the NO_2 distribution followed the same pattern. Furthermore, as a result of the concentration of the population in very specific points within the Spanish territory and the source of NO_2, mainly related to vehicle traffic, the distribution of this pollutant presented a wide range of values in the air, clearly differentiating between areas with a high population density and those without.

Just two weeks of lockdown measures and the mobility restrictions were reflected in a reduction of NO_2, mainly in those areas with larger populations. One month later, the NO_2 reduction was more evident, and not only in the populated areas, adopting a homogeneous distribution throughout the territory. The comparison between the NO_2 concentration values before and after the lockdown measures shows a strong relationship with the number of inhabitants.

These results should be taken into account by governments and policymakers to develop effective NO_2 emissions reduction and air pollution prevention policies. These policies should be based on adopting local measures within a global project.

Author Contributions: F.-J.M.-C., A.G.-F. and J.E.M.-L. conceived and designed the experiment, F.-J.M.-C., F.P.P. and P.T.-T. performed the experiment; F.-J.M.-C., F.P.P. and P.T.-T. analyzed the data and F.-J.M.-C. wrote the paper and A.G.-F. and J.E.M.-L. collaborated in the discussion of the results and revised the manuscript. All authors have read and agreed to the published version of the manuscript.

Funding: This research received no external funding.

Conflicts of Interest: The authors declare no conflict of interest.

References

1. World Health Organization Air pollution. Available online: https://www.who.int/health-topics/air-pollution#ta (accessed on 25 May 2020).
2. Gurjar, B.R.; Lelieveld, J. New Directions: Megacities and global change. *AtmEn* **2005**, *39*, 391–393. [CrossRef]
3. CAI-Asia Center. *Indonesia: Air Quality Profile*; Clean Air Initiative for Asian Cities (CAI-Asia) Center: Pasig, Philippines, 2010.
4. Khandelwal, S.; Goyal, R.; Kaul, N.; Mathew, A. Assessment of land surface temperature variation due to change in elevation of area surrounding Jaipur, India. *Egypt. J. Remote Sens. Space Sci.* **2018**, *21*, 87–94. [CrossRef]
5. Dadhich, P.N.; Hanaoka, S. Spatial investigation of the temporal urban form to assess impact on transit services and public transportation access. *Geo Spat. Inf. Sci.* **2012**, *15*, 187–197. [CrossRef]
6. Ravindra, K.; Mor, S.; Kamyotra, J.S.; Kaushik, C.P. Variation in Spatial Pattern of Criteria Air Pollutants Before and During Initial Rain of Monsoon. *Environ. Monit. Assess.* **2003**, *87*, 145–153. [CrossRef] [PubMed]
7. Marsh, W.M.; Grossa, J., Jr. *Environmental Geography: Science, Land Use, and Earth Systems*, 2nd ed.; John Wiley and Sons: New York, NY, USA, 2002; ISBN 0471503967.
8. Pasqua, L.A.; Damasceno, M.V.; Cruz, R.; Matsuda, M.; Martins, M.A.G.; Marquezini, M.V.; Lima-Silva, A.E.; Saldiva, P.H.N.; Bertuzzi, R. Exercising in the urban center: Inflammatory and cardiovascular effects of prolonged exercise under air pollution. *Chemosphere* **2020**, *254*, 126817. [CrossRef]
9. Shmuel, S.; White, A.J.; Sandler, D.P. Residential exposure to vehicular traffic-related air pollution during childhood and breast cancer risk. *Environ. Res.* **2017**, *159*, 257–263. [CrossRef]
10. Kopnina, H. Vehicular air pollution and asthma: Implications for education for health and environmental sustainability. *Local Environ.* **2017**, *22*, 38–48. [CrossRef]
11. Tang, G.; Zhao, P.; Wang, Y.; Gao, W.; Cheng, M.; Xin, J.; Li, X.; Wang, Y. Mortality and air pollution in Beijing: The long-term relationship. *Atmos. Environ.* **2017**, *150*, 238–243. [CrossRef]
12. He, G.; Fan, M.; Zhou, M. The effect of air pollution on mortality in China: Evidence from the 2008 Beijing Olympic Games. *J. Environ. Econ. Manag.* **2016**, *79*, 18–39. [CrossRef]
13. World Health Organization. *WHO Air Quality Guidelines for Particulate Matter, Ozone, Nitrogen Dioxide and Sulfur Dioxide: Global Update 2005: Summary of Risk Assessment*; World Health Organization: Geneva, Switzerland, 2006.
14. European Union Directive 2008/50/EC of the European Parliament and of the Council of 21 May 2008 on ambient air quality and cleaner air for Europe. *Off. J. Eur. Union* **2008**, *152*, 1–44.
15. Yebin, T.; Wei, H.; Xiaoliang, H.; Liuju, Z.; Shou-En, L.; Yi, L.; Lingzhen, D.; Yuanhang, Z.; Tong, Z. Estimated Acute Effects of Ambient Ozone and Nitrogen Dioxide on Mortality in the Pearl River Delta of Southern China. *Environ. Health Perspect.* **2012**, *120*, 393–398.
16. MacIntyre, E.A.; Gehring, U.; Mölter, A.; Fuertes, E.; Klümper, C.; Krämer, U.; Quass, U.; Hoffmann, B.; Gascon, M.; Brunekreef, B.; et al. Air Pollution and Respiratory Infections during Early Childhood: An Analysis of 10 European Birth Cohorts within the ESCAPE Project. *Environ. Health Perspect.* **2014**, *122*, 107–113. [CrossRef] [PubMed]
17. Hesterberg, T.W.; Bunn, W.B.; McClellan, R.O.; Hamade, A.K.; Long, C.M.; Valberg, P.A. Critical review of the human data on short-term nitrogen dioxide (NO_2) exposures: Evidence for NO_2 no-effect levels. *Crit. Rev. Toxicol* **2009**, *39*, 743–781. [CrossRef] [PubMed]
18. Ilan, L.; Cristian, M.; Gang, L.; Julie, N.; Brook, J.R. Evaluating Multipollutant Exposure and Urban Air Quality: Pollutant Interrelationships, Neighborhood Variability, and Nitrogen Dioxide as a Proxy Pollutant. *Environ. Health Perspect.* **2014**, *122*, 65–72.
19. Stieb, D.M.; Burnett, R.T.; Smith-Doiron, M.; Brion, O.; Shin, H.H.; Economou, V. A New Multipollutant, No-Threshold Air Quality Health Index Based on Short-Term Associations Observed in Daily Time-Series Analyses. *J. Air Waste Manag. Assoc.* **2008**, *58*, 435–450. [CrossRef] [PubMed]
20. Filleul, L.; Rondeau, V.; Vandentorren, S.; Le Moual, N.; Cantagrel, A.; Annesi-Maesano, I.; Charpin, D.; Declercq, C.; Neukirch, F.; Paris, C.; et al. Twenty five year mortality and air pollution: Results from the French PAARC survey. *Occup. Environ. Med.* **2005**, *62*, 453–460. [CrossRef]

21. Chen, X.; Zhang, L.; Huang, J.; Song, F.; Zhang, L.; Qian, Z.; Trevathan, E.; Mao, H.; Han, B.; Vaughn, M.; et al. Long-term exposure to urban air pollution and lung cancer mortality: A 12-year cohort study in Northern China. *Sci. Total Environ.* **2016**, *571*, 855–861. [CrossRef]
22. Gauderman, W.J.; Avol, E.; Lurmann, F.; Kuenzli, N.; Gilliland, F.; Peters, J.; McConnell, R. Childhood Asthma and Exposure to Traffic and Nitrogen Dioxide. *Epidemiology* **2005**, *16*, 737–743. [CrossRef]
23. Kowalska, M.; Skrzypek, M.; Kowalski, M.; Cyrys, J. Effect of NOx and NO_2 Concentration Increase in Ambient Air to Daily Bronchitis and Asthma Exacerbation, Silesian Voivodeship in Poland. *Int. J. Environ. Res. Public Health* **2020**, *17*, 754. [CrossRef]
24. Beelen, R.; Hoek, G.; Van Den Brandt, P.A.; Goldbohm, R.A.; Fischer, P.; Schouten, L.J.; Jerrett, M.; Hughes, E.; Armstrong, B.; Brunekreef, B. Long-Term Effects of Traffic-Related Air Pollution on Mortality in a Dutch Cohort (NLCS-AIR Study). *Environ. Health Perspect.* **2008**, *116*, 196–202. [CrossRef]
25. Eum, K.-D.; Kazemiparkouhi, F.; Wang, B.; Manjourides, J.; Pun, V.; Pavlu, V.; Suh, H. Long-term NO_2 exposures and cause-specific mortality in American older adults. *Environ. Int.* **2019**, *124*, 10–15. [CrossRef] [PubMed]
26. Amorim, L.C.A.; Carneiro, J.P.; Cardeal, Z.L. An optimized method for determination of benzene in exhaled air by gas chromatography–mass spectrometry using solid phase microextraction as a sampling technique. *J. Chromatogr. B* **2008**, *865*, 141–146. [CrossRef] [PubMed]
27. Ma, Y.; Richards, M.; Ghanem, M.; Guo, Y.; Hassard, J. Air pollution monitoring and mining based on sensor grid in London. *Sensors* **2008**, *8*, 3601–3623. [CrossRef] [PubMed]
28. Richards, M.; Ghanem, M.; Osmond, M.; Guo, Y.; Hassard, J. Grid-based analysis of air pollution data. *Ecol. Model.* **2006**, *194*, 274–286. [CrossRef]
29. Boubrima, A.; Bechkit, W.; Rivano, H. Optimal WSN Deployment Models for Air Pollution Monitoring. *IEEE Trans. Wirel. Commun.* **2017**, *16*, 2723–2735. [CrossRef]
30. Patil, D.; Thanuja, T.C.; Melinamath, B.C. *Air Pollution Monitoring System Using Wireless Sensor Network (WSN) BT-Data Management, Analytics and Innovation*; Balas, V.E., Sharma, N., Chakrabarti, A., Eds.; Springer: Singapore, 2019; pp. 391–400.
31. Yi, W.Y.; Lo, K.M.; Mak, T.; Leung, K.S.; Leung, Y.; Meng, M.L. A survey of wireless sensor network based air pollution monitoring systems. *Sensors* **2015**, *15*, 31392–31427. [CrossRef]
32. Zheng, Z.; Yang, Z.; Wu, Z.; Marinello, F. Spatial Variation of NO_2 and Its Impact Factors in China: An Application of Sentinel-5P Products. *Remote Sens.* **2019**, *11*, 1939. [CrossRef]
33. Nate, S. Remote-Sensing Applications for Environmental Health Research. *Environ. Health Perspect.* **2014**, *122*, A268–A275.
34. Burrows, J.P.; Weber, M.; Buchwitz, M.; Rozanov, V.; Ladstätter-Weißenmayer, A.; Richter, A.; DeBeek, R.; Hoogen, R.; Bramstedt, K.; Eichmann, K.-U.; et al. The Global Ozone Monitoring Experiment (GOME): Mission Concept and First Scientific Results. *J. Atmos. Sci.* **1999**, *56*, 151–175. [CrossRef]
35. Bovensmann, H.; Burrows, J.P.; Buchwitz, M.; Frerick, J.; Noël, S.; Rozanov, V.V.; Chance, K.V.; Goede, A.P.H. SCIAMACHY: Mission Objectives and Measurement Modes. *J. Atmos. Sci.* **1999**, *56*, 127–150. [CrossRef]
36. Callies, J.; Corpaccioli, E.; Eisinger, M.; Hahne, A.; Lefebvre, A. GOME-2-Metop's second-generation sensor for operational ozone monitoring. *ESA Bull.* **2000**, *102*, 28–36.
37. Levelt, P.F.; Van Den Oord, G.H.J.; Dobber, M.R.; Malkki, A.; Visser, H.; De Vries, J.; Stammes, P.; Lundell, J.O.V.; Saari, H. The ozone monitoring instrument. *IEEE Trans. Geosci. Remote Sens.* **2006**, *44*, 1093–1101. [CrossRef]
38. Veefkind, J.P.; Aben, I.; McMullan, K.; Förster, H.; De Vries, J.; Otter, G.; Claas, J.; Eskes, H.J.; De Haan, J.F.; Kleipool, Q.; et al. TROPOMI on the ESA Sentinel-5 Precursor: A GMES mission for global observations of the atmospheric composition for climate, air quality and ozone layer applications. *Remote Sens. Environ.* **2012**, *120*, 70–83. [CrossRef]
39. Griffin, D.; Zhao, X.; McLinden, C.A.; Boersma, F.; Bourassa, A.; Dammers, E.; Degenstein, D.; Eskes, H.; Fehr, L.; Fioletov, V.; et al. High-Resolution Mapping of Nitrogen Dioxide With TROPOMI: First Results and Validation Over the Canadian Oil Sands. *Geophys. Res. Lett.* **2019**, *46*, 1049–1060. [CrossRef]
40. Lamsal, L.N.; Duncan, B.N.; Yoshida, Y.; Krotkov, N.A.; Pickering, K.E.; Streets, D.G.; Lu, Z.U.S. NO_2 trends (2005–2013): EPA Air Quality System (AQS) data versus improved observations from the Ozone Monitoring Instrument (OMI). *Atmos. Environ.* **2015**, *110*, 130–143. [CrossRef]

41. Van Geffen, J.H.G.M.; Eskes, H.J.; Boersma, K.F.; Maasakkers, J.D.; Veefkind, J.P. TROPOMI ATBD of the Total and Tropospheric NO_2 Data Products. *Minist. Infrastruct. Water Manag.* **2019**. Available online: https://sentinel.esa.int/documents/247904/2476257/Sentinel-5P-TROPOMI-ATBD-NO2-data-products (accessed on 10 January 2020).
42. Curier, R.L.; Kranenburg, R.; Segers, A.J.S.; Timmermans, R.M.A.; Schaap, M. Synergistic use of OMI NO_2 tropospheric columns and LOTOS–EUROS to evaluate the NOx emission trends across Europe. *Remote Sens. Environ.* **2014**, *149*, 58–69. [CrossRef]
43. Castellanos, P.; Boersma, K.F. Reductions in nitrogen oxides over Europe driven by environmental policy and economic recession. *Sci. Rep.* **2012**, *2*, 265. [CrossRef]
44. Ghude, S.D.; Pfister, G.G.; Jena, C.; Van Der A, R.J.; Emmons, L.K.; Kumar, R. Satellite constraints of nitrogen oxide (NOx) emissions from India based on OMI observations and WRF-Chem simulations. *Geophys. Res. Lett.* **2013**, *40*, 423–428. [CrossRef]
45. Streets, D.G.; Canty, T.; Carmichael, G.R.; De Foy, B.; Dickerson, R.R.; Duncan, B.N.; Edwards, D.P.; Haynes, J.A.; Henze, D.K.; Houyoux, M.R.; et al. Emissions estimation from satellite retrievals: A review of current capability. *Atmos. Environ.* **2013**, *77*, 1011–1042. [CrossRef]
46. Wang, S.W.; Zhang, Q.; Streets, D.G.; He, K.B.; Martin, R.V.; Lamsal, L.N.; Chen, D.; Lei, Y.; Lu, Z. Growth in NOx emissions from power plants in China: Bottom-up estimates and satellite observations. *Atmos. Chem. Phys.* **2012**, *12*, 4429. [CrossRef]
47. Kim, S.-W.; Heckel, A.; McKeen, S.A.; Frost, G.J.; Hsie, E.-Y.; Trainer, M.K.; Richter, A.; Burrows, J.P.; Peckham, S.E.; Grell, G.A. Satellite-Observed U.S. Power Plant NOx Emission Reductions and Their Impact on Air Quality. *Geophys. Res. Lett.* **2006**, *33*. Available online: https://agupubs.onlinelibrary.wiley.com/doi/full/10.1029/2006GL027749 (accessed on 20 May 2020). [CrossRef]
48. World Economic Forum The Global Risks Report 2020. 2020. Available online: https://www.weforum.org/reports/the-global-risks-report-2020 (accessed on 20 May 2020).
49. Ye, Z.-W.; Yuan, S.; Yuen, K.-S.; Fung, S.-Y.; Chan, C.-P.; Jin, D.-Y. Zoonotic origins of human coronaviruses. *Int. J. Biol. Sci.* **2020**, *16*, 1686–1697. [CrossRef]
50. Ahmad, T.; Khan, M.; Haroon, T.H.M.; Nasir, S.; Hui, J.; Bonilla-Aldana, D.K.; Rodriguez-Morales, A.J. COVID-19: Zoonotic aspects. *Travel Med. Infect. Dis.* **2020**. [CrossRef] [PubMed]
51. Mackenzie, J.S.; Chua, K.B.; Daniels, P.W.; Eaton, B.T.; Field, H.E.; Hall, R.A.; Halpin, K.; Johansen, C.A.; Kirkland, P.D.; Lam, S.K.; et al. Emerging viral diseases of Southeast Asia and the Western Pacific. *Emerg. Infect. Dis.* **2001**, *7*, 497–504. [CrossRef] [PubMed]
52. Olsen, B.; Munster, V.J.; Wallensten, A.; Waldenström, J.; Osterhaus, A.D.M.E.; Fouchier, R.A.M. Global Patterns of Influenza a Virus in Wild Birds. *Science* **2006**, *312*, 384–388. [CrossRef] [PubMed]
53. Fergus, R.; Fry, M.; Karesh, W.B.; Marra, P.P.; Newman, S.; Paul, E. Migratory Birds and Avian Flu. *Science* **2006**, *312*, 845–846. [CrossRef]
54. Petersen, L.R.; Marfin, A.A. Shifting Epidemiology of Flaviviridae. *J. Travel Med.* **2008**, *12*, s3–s11. [CrossRef]
55. Leviston, Z.; Leitch, A.; Greenhill, M.; Leonard, R.; Walker, I. Australians' Views of Climate Change. *Canberra CSIRO* **2011**. Available online: https://www.researchgate.net/profile/Anne_Leitch/publication/255960321_Australians\T1\textquoteright_Views_of_Climate_Change/links/00b49520f2ef390d88000000/Australians-Views-of-Climate-Change.pdf (accessed on 20 May 2020).
56. Price, J.C.; Walker, I.A.; Boschetti, F. Measuring cultural values and beliefs about environment to identify their role in climate change responses. *J. Environ. Psychol.* **2014**, *37*, 8–20. [CrossRef]
57. Van Der Linden, S.L.; Leiserowitz, A.A.; Feinberg, G.D.; Maibach, E.W. The Scientific Consensus on Climate Change as a Gateway Belief: Experimental Evidence. *PLoS ONE* **2015**, *10*, e0118489. [CrossRef]
58. Callaway, E. Time to use the p-word? Coronavirus enter dangerous new phase. *Nature* **2020**, *579*, 10–38. [CrossRef]
59. Remuzzi, A.; Remuzzi, G. COVID-19 and Italy: What next? *Lancet* **2020**, *395*, 1225–1228. [CrossRef]
60. Hou, C.; Chen, J.; Zhou, Y.; Hua, L.; Yuan, J.; He, S.; Guo, Y.; Zhang, S.; Jia, Q.; Zhao, C.; et al. The effectiveness of quarantine of Wuhan city against the Corona Virus Disease 2019 (COVID-19): A well-mixed SEIR model analysis. *J. Med. Virol.* **2020**, *92*, 841–848. [CrossRef] [PubMed]
61. Lau, H.; Khosrawipour, V.; Kocbach, P.; Mikolajczyk, A.; Schubert, J.; Bania, J.; Khosrawipour, T. The positive impact of lockdown in Wuhan on containing the COVID-19 outbreak in China. *J. Travel Med.* **2020**, *27*. [CrossRef] [PubMed]

62. Peto, J.; Alwan, N.A.; Godfrey, K.M.; Burgess, R.A.; Hunter, D.J.; Riboli, E.; Romer, P. Universal weekly testing as the UK COVID-19 lockdown exit strategy. *Lancet* **2020**, *395*, 1420–1421. [CrossRef]
63. Gorelick, N.; Hancher, M.; Dixon, M.; Ilyushchenko, S.; Thau, D.; Moore, R. Google Earth Engine: Planetary-scale geospatial analysis for everyone. *Remote Sens. Environ.* **2017**, *202*, 18–27. [CrossRef]
64. Eskes, H.J.; Eichmann, K.U. S5P Mission Performance Centre Nitrogen Dioxide [L2__NO2___]. 2019. Available online: https://sentinel.esa.int/documents/247904/3541451/Sentinel-5P-Nitrogen-Dioxide-Level-2-Product-Readme-File (accessed on 15 June 2020).
65. Degraeuwe, B.; Pisoni, E.; Peduzzi, E.; De Meij, A.; Monforti-Ferrario, F.; Bodis, K.; Mascherpa, A.; Astorga-Llorens, M.; Thunis, P.; Vignati, E. *Urban NO_2 Atlas*; Publications Office of the European Union: Brussels, Belgium, 2019; ISBN 978-92-76-10386-8.
66. Harapan, H.; Itoh, N.; Yufika, A.; Winardi, W.; Keam, S.; Te, H.; Megawati, D.; Hayati, Z.; Wagner, A.L.; Mudatsir, M. Coronavirus disease 2019 (COVID-19): A literature review. *J. Infect. Public Health* **2020**, *13*, 667–673. [CrossRef]
67. Ficetola, G.F.; Rubolini, D. Climate affects global patterns of COVID-19 early outbreak dynamics. *MedRxiv* **2020**. [CrossRef]
68. Zhu, Y.; Price, O.R.; Kilgallon, J.; Qi, Y.; Tao, S.; Jones, K.C.; Sweetman, A.J. Drivers of contaminant levels in surface water of China during 2000–2030: Relative importance for illustrative home and personal care product chemicals. *Environ. Int.* **2018**, *115*, 161–169. [CrossRef]
69. Zhu, Y.; Zhan, Y.; Wang, B.; Li, Z.; Qin, Y.; Zhang, K. Spatiotemporally mapping of the relationship between NO_2 pollution and urbanization for a megacity in Southwest China during 2005–2016. *Chemosphere* **2019**, *220*, 155–162. [CrossRef]
70. De Tráfico, D.G.; Del, I.M. Evolución del Tráfico por el efecto COVID-19. Available online: http://www.dgt.es/Galerias/covid-19/Evolucion-Intensidades-dia-02-04-2020-Periodo-Coronavirus.pdf (accessed on 9 May 2020).
71. Banister, D. Energy, quality of life and the environment: The role of transport. *Transp. Rev.* **1996**, *16*, 23–35. [CrossRef]
72. Camagni, R.; Gibelli, M.C.; Rigamonti, P. Urban mobility and urban form: The social and environmental costs of different patterns of urban expansion. *Ecol. Econ.* **2002**, *40*, 199–216. [CrossRef]
73. Ambarwati, L.; Verhaeghe, R.; Van Arem, B.; Pel, A.J. The influence of integrated space–transport development strategies on air pollution in urban areas. *Transp. Res. Part D Transp. Environ.* **2016**, *44*, 134–146. [CrossRef]